C. E. KENNETH MEES OBSERVATORY

UNIVERSITY OF ROCHESTER
ROCHESTER, N.Y.

REPRINT NO. 14

LATE PHASES OF STELLAR EVOLUTION. I. PURE IRON STARS

By

M. P. SAVEDOFF, H. M. VAN HORN, AND S. C. VILA

Reprinted from THE ASTROPHYSICAL JOURNAL Vol. 155, No. 1, Part 1, January 1969

THE ASTROPHYSICAL JOURNAL, Vol. 155, January 1969

LATE PHASES OF STELLAR EVOLUTION. I. PURE IRON STARS

M. P. SAVEDOFF, H. M. VAN HORN, AND S. C. VILA*
Department of Physics and Astronomy and C. E. Kenneth Mees
Observatory, University of Rochester
Received June 3, 1968; revised July 1, 1968

ABSTRACT

The effect of neutrino loss on the evolution of pure iron stars of 0.398, 0.631, 1.0, and 2.5 $M_\odot$ is studied. The evolutionary tracks, computed by the Henyey-Schwarzschild method, are followed into the white-dwarf stage, in the case of those models less massive than the Chandrasekhar limit, or to the stage of incipient instability in the case of the presupernova models. Comparison with other models for similar evolutionary phases enables us to identify some of the physical processes of importance for these late stages and to suggest the following conclusions: (1) the 1 $M_\odot$ models with neutrino losses follow an evolutionary path resembling the one suggested by Harmon and Seaton for the nuclei of the planetary nebulae and are also consistent with the time scale of ~10000 years suggested for these stars; (2) the iron-helium transition may not be the mechanism responsible for the core collapse in presupernovae of mass ~2.5 $M_\odot$.

I. INTRODUCTION

This paper is the first in a series dealing with the late phases of stellar evolution. Our aim is to investigate the range of conditions over which the various physical processes that are important in these stages dominate the evolution and to establish the scale of these processes. The present calculations are concerned with the evolutionary paths of homogeneous stellar models starting from arbitrary but reasonable initial conditions. As we shall show, only the first portions of these tracks are affected by the choice of starting model. Since we treat the physics rather accurately—within the limitations of these simplifying approximations—the conditions in the deep interiors can provide insight into conditions in real stars, so that our results can be used to guide calculations of more realistic model sequences.

A numerical investigation of pure iron stars of 1.0 and 2.5 $M_\odot$, both with and without neutrino losses, has previously been carried out by Vila (1965). We have now extended these calculations to 0.398 and 0.631 $M_\odot$, and we present here a discussion of the results for all four cases. The choice of an iron composition was made both because it represents one possible extreme of composition and because nuclear reactions do not have to be considered. Furthermore, in the case of the 2.5 $M_\odot$ models this choice enables us to study the evolution of presupernova models immediately prior to the iron-helium transition, but still in the regime in which dynamical effects can be neglected.

II. METHOD OF MODEL CONSTRUCTION

a) The Program

The calculations were carried out using the method of Henyey and his co-workers (1959, 1964) with the logarithmic variables discussed by Schwarzschild (1958, p. 116) and by Härm and Schwarzschild (1964). Each model consisted of about 100 shells with masses determined by the condition that the change in the logarithm of P, r, M_r be less than 0.1. The time step was chosen so that the change in log T per iteration was below 0.0001 for all shells after about 10 iterations. The computations were carried out on an IBM 7074 at the University of Rochester and on an IBM 7090 at Imperial College, London, and required approximately 1 minute per model.

* Present address: Goddard Institute for Space Studies, NASA, New York, N.Y.

b) Surface Boundary Condition

Most of the models we have calculated have made use of the "radiative-zero" surface boundary condition described by Schwarzschild (1958, p. 89). In the calculations of the 0.631 and 0.398 $M_\odot$ models this condition was modified as follows. The opacity law was assumed to have the form of a generalized Kramers' law: $K = K_0 P^a T^{-S}$, where K_0, a, and S are all determined at the last mass shell before the surface (for Kramers' opacity $a = 1$ and $S = 4.5$), and the ratio β of gas pressure to total pressure was taken to be of the form $\beta = \beta_0(P/T^4)^\epsilon$, where β_0 and ϵ are determined at the last mass shell. Since $\epsilon \equiv (1 - \beta)/\beta$, $\epsilon \ll 1$ in the usual situation where the radiation pressure is negligible, and β_0 is, therefore, also almost unity. Under these circumstances Schwarzschild's (1958, p. 89) equation (11.5) is replaced by

$$P = \left(\frac{1 + a}{4 + S}\frac{4ac}{3}\frac{4\pi GM}{K_0 L}\right)^{1/(1+a)} T^{(4+S)/(1+a)}, \tag{1}$$

and equation (14.5) is replaced by the system of equations

$$Y \equiv \frac{k}{GM\mu H}\frac{S + 4 + a}{\beta(1 + a)} rT, \tag{2}$$

$$\Im \equiv (1 - Y)^C\left[1 + \sum_{n=1}^{6}\frac{(C + 1)(C + 2) \ldots (C + n)}{n!}\frac{C + 4}{C + 4 + n} Y^n\right]; \tag{3}$$

$$C \equiv \frac{S - 3a}{1 + a},$$

$$\tfrac{1}{2}\left(1 - \frac{M_r^2}{M^2}\right) \simeq \frac{4\pi r^4 P}{GM^2}\Im, \tag{4}$$

where $Y = 1 - r/R$, and $\Im$ is the integral which arises in the solution of the mass-conservation equation in the envelope. Here r/R is the ratio of the radius of the last shell to the total radius of the star. Equation (1) then provides the boundary condition on the luminosity L to be used at the last shell, and equation (4)—with M_r held fixed during the relaxation phase of the calculations but variable from one evolutionary model to the next, and with the help of equations (2) and (3)—provides the boundary relation for R. The characteristics of models which were calculated with the new surface condition were not appreciably different from those computed using Schwarzschild's "radiative-zero" method; the models with either surface condition followed the same locus in the (log L, log T_e)-diagram but at slightly different time scales (~5 per cent).

c) Equation of State, Opacity, and Neutrino Rates

We took the pressure P and the temperature T as the two independent variables which characterize the thermodynamic state of matter in the stellar interior; we therefore require the entropy per gram, S, and the density ρ as functions of P and T. We treat the ions as a perfect gas throughout; electrostatic corrections at low temperatures (Salpeter 1961) and the transition to the crystalline phase (Van Horn 1968) were not taken into account. The pressure, temperature, density, and entropy are therefore related exactly as in § 3A.1 of Hayashi *et al.* (1962), and we have approximated then contribution of the electrons—as given by the numerical calculations of Grasberger (1961)—by piecewise continuous functions which give log ρ and the electron entropy S_e as functions of P and T to 5 per cent accuracy over the entire range of the variables. We assume complete ionization throughout the star. Since this is invalid only if both $T \ll 10^8$ ° K *and* $\rho \ll 10^5$ g cm^{-3}, we obtain an inaccurate temperature profile only in the outermost 10 per cent of the total mass even in the most extreme case of the 0.398 $M_\odot$ star.

For the opacities and neutrino rates we have used piecewise continuous functions which give an accuracy of 5 per cent over the needed range. For the electron-scattering opacity we have used equations (3A.32) and (3A.33) of Hayashi *et al.* (1962), and for the conductive opacity, the values given in the numerical tabulation by Mestel (1950). The free-free opacity was determined by fitting an expression of the form (Hayashi *et al.* 1962, eq. [3A.44])

$$K_{ff} = K_1 \frac{1}{T^2} \ln \frac{e^{\psi} + 1}{e^{\psi - 7} + 1}, \tag{5}$$

where ψ is the degeneracy parameter of Hayashi *et al.*, to a table of pure iron opacities which was kindly provided for us by Dr. A. N. Cox of the Los Alamos Scientific Laboratory. Fitting with his table at $T = 4 \times 10^7$ ° K, $\rho = 60$ g cm^{-3} we obtained $K_1 = 4.193 \times 10^{17}$. The corresponding value of K_0, which occurs in Kramers' opacity formula is 2.43×10^{25}.

At the high densities and low temperatures encountered in the phases in which we are interested only three neutrino processes are important. For the *photoneutrino* rate we have used equation (2F.24) of Hayashi *et al.* (1962). This yields a gross overestimate of the rate when the electrons are highly degenerate, but since under these conditions this process turns out not to contribute very much to the total neutrino-loss rate the error is not serious. For the *pair-annihilation* process we have used the expression (Hayashi *et al.* 1962, § 2F.2b)

$$\log \epsilon_{\mathrm{pa}} = 18.7 + 3 \log T_9 - 5.15\, T_9^{-1} - \log \rho, \tag{6}$$

where ϵ_{pa} is the rate of energy loss in ergs g^{-1} sec^1, T_9 is the temperature in units of 10^9 ° K, and ρ is the density in g cm^{-3}. The rate of energy loss due to *plasma neutrinos* has been tabulated by Inman and Ruderman (1964). We have *not* corrected the plasma rates by the factor of $\frac{1}{4}$ discussed by Zaidi (1965), which became known to us after the 1 $M_\odot$ case had been completed.

Since all of these neutrino-loss mechanisms depend upon the existence in fact of the theoretically predicted direct electron-neutrino interaction (Sudarshan and Marshak 1958; Feynman and Gell-Mann 1958), which has not yet been established experimentally, we have calculated two parallel sets of evolutionary model sequences both with and without the inclusion of these processes of neutrino loss.

d) Starting the Integrations

The starting model for the 1 $M_\odot$ sequence was a polytrope of index $n = 3$ and with the central density given by $\log \rho_c = 3.435$, $\log T_c = 8.085$, $\log P_c = 19.126$, $\log R = 10.400$, all in cgs units. At these temperatures and densities both neutrino losses and deviations from the perfect-gas laws are negligible. The luminosity distribution was normalized to an arbitrary value of the total luminosity L at the surface, and L was varied until convergence was obtained. In the 1 $M_\odot$ case the value $L = 112.8\, L_\odot$ proved satisfactory.

For the 2.5 $M_\odot$ sequences the starting model was taken to be a polytrope of index $n = 3$, but with $\log \rho_c = 2.738$, $\log T_c = 8.038$, $\log P_c = 18.495$, $\log R = 10.742$, and $L = 3.74 \times 10^3\, L_\odot$.

For the sequences of lower mass satisfactory starting models were obtained by means of isentropic homology transformations from the early relaxed 1 $M_\odot$ models.

Although the initial models are artificially contrived, the starting transients damp out in times of the order of the photon diffusion time

$$\tau_{\mathrm{ph}} \sim K\rho R^2/c \tag{7}$$

where K, ρ, and R are typical values for the opacity, mass density, and radius, respectively, and c is the velocity of light. The models with ages $t > \tau_{\mathrm{ph}}$ are thus independent

of the initial conditions. The recent computations of pre-main-sequence evolution by Bodenheimer (1966) graphically demonstrate the independence of phases with ages $t > \tau_{ph}$ from the initial conditions for some rather extreme choices for the starting model. Initial photon-diffusion time scales for our 0.398, 0.631, and 1.0 $M_\odot$ models are, respectively, 1.2×10^5, 2.5×10^5, 4.6×10^5 years, all of which are shorter than the corresponding times, 3.1×10^7, 3.7×10^6, and 5.5×10^5 years, at which the peak luminosity is reached in the models which include neutrino losses (see Fig. 1). In the 2.5 $M_\odot$ case, τ_{ph} is of the order of the entire evolutionary age of the star. For this case, we cannot make very strong statements about the relevance of our calculations, and we have simply followed the philosophy outlined in § I.

III. PRE-WHITE-DWARF EVOLUTION

The evolutionary tracks of our pre-white-dwarf models are shown in Figure 1. The wiggles at the beginning of each track are starting transients which damp out in times

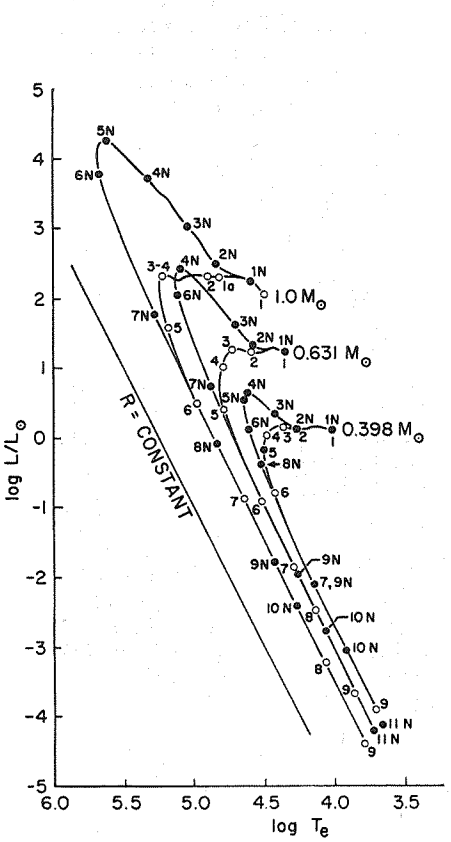

FIG. 1

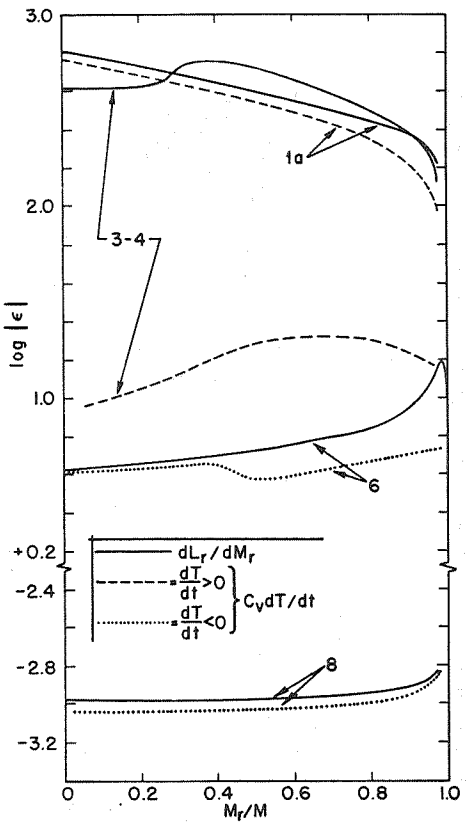

FIG. 2

FIG. 1.—H-R diagram for pure iron stars of 0.398, 0.631, and 1.0 $M_\odot$ with neutrino losses (*filled circles* and numbers with suffix *N*) and without (*open circles* and numbers without suffix). Numbered points refer to specific models in Tables 1–6.

FIG. 2.—Distributions of net gravitational-energy generation and of the storage or release of heat at constant volume as functions of the fractional mass M_r/M for several stages in the evolution of the 1 $M_\odot$ star without neutrino losses. C_v is the specific heat per gram at constant volume. Numbers refer to specific models listed in Table 1.

of the order of τ_{ph}. In Tables 1–6 we give for the models referenced by the numbered points the quantities ρ, T, P, etc., all in cgs units. The subscripts c, d, pk refer, respectively, to the mass shells where $M_r = 0$, $\psi(M_r) = 0$, $dT/dM_r = 0$. We discuss separately the evolution in the two cases with and without neutrino losses.

a) Evolution without Neutrino Loss

The evolution of neutrinoless models proceeds as discussed in § 9 of Hayashi *et al.* (1962). The initial phase is one of quasi-homologous contraction that takes place at almost constant luminosity. This is a consequence of the importance of electron scattering in the opacity law during these early stages. Degeneracy appears in the center at model 2($\psi_c \approx 0$), and the mass fraction contained in the degenerate core grows rapidly until at model 4 it extends over approximately 90 per cent of the mass of the star, at which stage the maximum of the central temperature is reached. The evolution from models 5–9 covers the final cooling, down a line of almost constant radius to the region occupied by the observed white dwarfs ($\log L/L_\odot \leq -2$).

The distribution of gravitational-energy release is shown in Figure 2 for several of the 1 $M_\odot$ models without neutrino loss. In the early evolution (models 1–4) about half of the total energy released is stored as thermal energy of the electrons and ions. The rest of the gravitational energy liberated goes partly into raising the Fermi level of the electrons, and the balance gives rise to the luminous energy flux. At the point where the central temperature reaches its maximum value, however, the further, slower compression of the central regions cannot alone maintain the rate of energy loss there, and the deficiency is made up from the thermal energy store of the matter at the center; the heat *loss* ($C_v dT/dt$; $dT/dt < 0$) is shown in the figure. At the temperature maximum (model 3–4) the magnitude of $C_v dT/dt$ is small in comparison with the net gravitational-energy release, as would be expected, since this model represents a transition from the contraction phase to the cooling phase of the evolution. (The wiggle in dL_r/dM_r at $M_r/M \sim 0.3$ is related to the transition from non-relativistic to relativistic degeneracy in the 1 $M_\odot$ model with the associated changes in the equation of state.)

During the final cooling phases the gravitational-energy release is highest in the outer layers, where the contraction proceeds most rapidly. This is clearly shown in model 6 of Figure 2, where virtually all the energy loss in the relativistic, degenerate inner core ($M_r/M \lesssim 0.45$) is due to heat leakage, while ~30 per cent of the luminosity in the outer layers is still due to gravitational contraction. Finally, in model 8 the cooling of the degenerate core accounts for ~90 per cent of the total luminosity, in agreement with the result of Mestel and Ruderman (1967). The temperature distribution in the degenerate core in all of these cooling phases is very nearly uniform because of the high efficiency of thermal conduction by the degenerate electrons (Fig. 3).

These numerical calculations may be compared instructively with the simplified evolutionary model discussed by Schwarzschild (1958, p. 237). As Schwarzschild shows, for a white dwarf with an isothermal core and a radiative envelope in which the opacity is given by Kramers' law, the luminosity L is proportional to $T_c^{3.5}$. The present model sequence shows $L \propto T_c^{2.63 \pm 0.02}$, where the uncertainty in the exponent reflects mainly the uncertainties in the approximations used for the various functions of state (K, ϵ, etc.). The differences in the exponents are due to departures of the opacity from Kramers' law: For a generalized Kramers' opacity of the form $K \propto P^a T^{-S}$ the generalization of Schwarzschild's equation (27.5) is $L \propto T_{tr}^{(1.5+S-2.5a)} \equiv T_{tr}^n$, where T_{tr} is the temperature at the transition layer defined by

$$\log T_{tr} - \tfrac{2}{3} \log \rho_{tr} = 4.6 . \qquad (8)$$

For our sequences, the exponent n at this transition layer is 2.42 ± 0.02 and n increases to 3.25 at the surface. Accordingly a relationship like Schwarzschild's equation (27.5)

TABLE I

Properties of 1 $M_\odot$ Models Without Neutrino Loss

No.	Age	log ρ_c	log T_c	log P_c	ψ_c	log ρ_d	log T_d	log P_d	M_r/M	r_d/R	log $L/L_\odot$	log T_e	$R/R_\odot$
1	0 years	3.435	8.085	19.126	-2.14	---	---	---	---	---	2.053	4.498	3.61×10^{-1}
1a	6.849×10^{5}	4.759	8.543	20.946	-0.63	---	---	---	---	---	2.308	4.813	1.13×10^{-1}
2	1.133×10^{6}	5.219	8.678	21.553	+0.03	---	---	---	---	---	2.307	4.893	7.85×10^{-2}
3-4	4.986×10^{6}	7.092	9.088	24.066	4.80	5.124	8.625	21.402	0.952	0.580	2.317	5.220	1.76×10^{-2}
5	1.272×10^{7}	7.764	8.870	24.972	35.6	4.708	8.377	20.735	0.998	0.840	1.576	5.194	8.46×10^{-3}
6	2.942×10^{7}	7.939	8.481	25.206	120	4.285	8.070	20.009	1.000	0.930	0.495	4.977	6.60×10^{-3}
7	8.222×10^{7}	7.947	7.963	25.217	390	3.637	7.632	18.940	1.000	0.973	-0.899	4.644	6.18×10^{-3}
8	7.772×10^{8}	7.948	7.071	25.217	3×10^{3}	2.275	6.828	16.759	1.000	0.996	-3.246	4.063	6.01×10^{-3}
9	3.079×10^{9}	7.948	6.636	25.217	2×10^{5}	---	---	---	---	---	-4.367	3.783	6.00×10^{-3}

TABLE 2

Properties of 0.631 $M_\odot$ Models Without Neutrino Loss

No.	Age	log ρ_c	log T_c	log P_c	ψ_c	log ρ_d	log T_d	log P_d	M_r/M	r_d/R	log $L/L_\odot$	log T_e	$R/R_\odot$
1	0 years	3.464	8.005	19.074	-1.80	---	---	---	---	---	1.226	4.341	2.88×10^{-1}
2	3.96×10^{6}	4.811	8.414	20.878	+0.09	---	---	---	---	---	1.248	4.598	9.04×10^{-2}
3	7.80×10^{6}	5.522	8.612	21.841	1.37	4.770	8.388	20.810	0.580	0.314	1.261	4.726	5.08×10^{-2}
4	1.77×10^{7}	6.179	8.675	22.718	3.98	4.573	8.277	20.500	0.925	0.562	1.001	4.797	2.72×10^{-2}
5	5.00×10^{7}	6.795	8.475	23.568	14.9	4.220	8.068	19.937	0.953	0.800	0.378	4.779	1.44×10^{-2}
6	1.34×10^{8}	6.913	8.012	23.739	50.3	3.638	7.679	18.971	1.000	0.935	-0.910	4.514	1.11×10^{-2}
7	2.92×10^{8}	6.918	7.664	23.746	160	3.233	7.390	18.284	1.000	0.963	-1.857	4.290	1.04×10^{-2}
8	5.00×10^{8}	6.918	7.426	23.746	280	2.874	7.172	17.708	1.000	0.979	-2.494	4.135	1.03×10^{-2}
9	1.78×10^{9}	6.918	6.977	23.747	780	2.244	6.765	16.670	1.000	0.992	-3.678	3.843	1.01×10^{-2}

TABLE 3

Properties of 0.398 $M_\odot$ Models Without Neutrino Loss

No.	Age	log ρ_c	log T_c	log P_c	ψ_c	log ρ_d	log T_d	log P_d	M_r/M	r_d/R	log $L/L_\odot$	log T_e	$R/R_\odot$
1	0 years	2.964	7.710	18.275	-1.94	---	---	---	---	---	0.105	4.015	3.54×10^{-1}
2	1.61×10^{7}	4.245	8.097	19.989	-0.11	---	---	---	---	---	0.132	4.258	1.20×10^{-1}
3	2.76×10^{7}	4.816	8.255	20.741	+0.90	4.276	8.097	20.022	0.403	0.248	0.154	4.357	7.76×10^{-2}
4	6.18×10^{7}	5.581	8.368	21.795	3.50	4.217	8.044	19.912	0.870	0.491	0.017	4.477	3.81×10^{-2}
5	9.47×10^{7}	5.855	8.325	22.192	6.04	4.148	7.990	19.790	0.949	0.601	-0.167	4.498	2.80×10^{-2}
6	1.92×10^{8}	6.098	8.101	22.537	14.5	3.741	7.764	19.156	0.994	0.790	-0.799	4.422	1.92×10^{-2}
7	5.16×10^{8}	6.179	7.631	22.652	54.7	3.119	7.354	18.129	1.000	0.924	-2.105	4.148	1.51×10^{-2}
9	2.67×10^{9}	6.182	6.954	22.657	265	2.222	6.750	16.633	1.000	0.981	-3.923	3.711	1.40×10^{-2}

TABLE 4

Properties of 1 $M_\odot$ Models With Neutrino Loss

No	Age	$\log\rho_c$	$\log T_c$	$\log P_c$	ψ_c	$\epsilon_{\upsilon,c}$	$\log\rho_{pk}$	$\log T_{pk}$	$\log P_{pk}$	ψ_{pk}	$\epsilon_{\upsilon,pk}$	$M_{r,pk}/M$	r_{pk}/R	$\log L_\upsilon/L_\odot$	$\log L/L_\odot$	$\log Te$	$R/R_\odot$
1N	0 years	3.731	8.209	19.550	-1.89	2.37×10^{1}	---	---	---	---	---	---	---	0.02	2.246	4.597	$2.86\times10^{+1}$
2N	4.290×10^{5}	4.930	8.500	21.082	+0.04	5.16×10^{3}	---	---	---	---	---	---	---	2.62	2.493	4.837	1.25×10^{-1}
3N	2904*	6.065	8.638	22.553	3.71	1.14×10^{5}	5.515	8.675	21.866	0.97	1.32×10^{5}	0.271	0.100	4.53	3.026	5.045	8.81×10^{-2}
4N	5374*	7.318	8.501	24.338	25.72	4.38×10^{5}	5.963	8.920	22.571	1.07	1.37×10^{7}	0.728	0.120	6.51	3.704	5.329	6.46×10^{-2}
5N	5945*	7.851	8.277	25.085	150	2.36×10^{4}	5.376	8.867	21.910	-0.41	5.19×10^{6}	0.976	0.240	5.48	4.256	5.626	2.53×10^{-2}
6N	6715*	7.905	8.206	25.159	210	4.87×10^{3}	5.455	8.795	21.911	+0.15	1.18×10^{6}	0.985	0.500	4.67	3.765	5.675	1.15×10^{-2}
7N	4.883×10^{5}	7.940	8.075	25.206	300	1.71×10^{2}	5.556	8.560	21.859	1.84	1.84×10^{4}	0.991	0.760	2.83	1.770	5.278	7.15×10^{-3}
8N	6.983×10^{5}	7.947	7.934	25.216	420	2.76×10^{0}	5.345	8.125	21.381	4.53	4.58×10^{1}	0.997	0.880	0.89	-0.0735	4.845	6.32×10^{-3}
9N	7.328×10^{6}	7.947	7.672	25.217	760	1.41×10^{-3}	---	---	---	---	---	---	---	-1.19	-1.772	4.429	6.08×10^{-3}
10N	1.090×10^{8}	7.947	7.392	25.217	1×10^{3}	6.86×10^{-6}	---	---	---	---	---	---	---	-3.55	-2.411	4.271	6.04×10^{-3}

* $+4.704\times10^{5}$ years

TABLE 5

Properties of 0.631 $M_\odot$ Models With Neutrino Loss

No	Age	$\log\rho_c$	$\log T_c$	$\log P_c$	ψ_c	$\epsilon_{\upsilon,c}$	$\log\rho_{pk}$	$\log T_{pk}$	$\log P_{pk}$	ψ_{pk}	$\epsilon_{\upsilon,pk}$	$M_{r,pk}/M$	r_{pk}/R	$\log L_\upsilon/L_\odot$	$\log L/L_\odot$	$\log Te$	$r/R_\odot$
1N	0 years	3.464	8.005	19.074	-1.80	5.51×10^{-1}	---	---	---	---	---	---	---	-1.78	1.226	4.341	2.88×10^{-1}
2N	2.59×10^{6}	4.643	8.327	20.620	+0.01	2.13×10^{2}	---	---	---	---	---	---	---	-1.10	1.320	4.569	1.12×10^{-1}
3N	3.25×10^{6}	5.313	8.409	21.464	1.85	1.20×10^{3}	5.127	8.416	21.224	1.10	1.18×10^{3}	0.084	0.093	2.03	1.602	4.703	8.37×10^{-2}
4N	7184*	6.603	8.057	23.280	31.0	6.05×10^{2}	5.254	8.560	21.479	0.74	1.58×10^{4}	0.805	0.280	3.52	2.434	5.103	3.45×10^{-2}
6N	55,162*	6.800	7.924	23.571	72.7	1.01×10^{2}	5.286	8.516	21.485	1.09	7.19×10^{3}	0.900	0.428	3.05	2.037	5.114	2.08×10^{-2}
7N	3.83×10^{6}	6.895	7.776	23.711	120	4.56×10^{0}	5.226	8.325	21.308	2.05	3.00×10^{2}	0.958	0.644	1.58	0.725	4.882	1.34×10^{-2}
9N	1.99×10^{7}	6.918	7.556	23.746	200	1.21×10^{-2}	---	---	---	---	---	---	---	-1.19	-1.970	4.263	1.04×10^{-2}
10N	2.03×10^{8}	6.918	7.320	23.746	350	5.71×10^{-6}	---	---	---	---	---	---	---	-3.20	-2.780	4.064	1.02×10^{-2}
11N	2.50×10^{9}	6.918	6.767	23.747	1×10^{3}	6.88×10^{-11}	---	---	---	---	---	---	---	-8.47	-4.228	3.706	1.00×10^{-2}

* $+3.50\times10^{6}$ years

TABLE 6

Properties of 0.398 $M_\odot$ Models With Neutrino Loss

No	Age	$\log\rho_c$	$\log T_c$	$\log P_c$	ψ_c	$\epsilon_{\upsilon,c}$	$\log\rho_{pk}$	$\log T_{pk}$	$\log P_{pk}$	ψ_{pk}	$\epsilon_{\upsilon,pk}$	$M_{r,pk}/M$	r_{pk}/R	$\log L_\upsilon/L_\odot$	$\log L/L_\odot$	$\log T_e$	$R/R_\odot$
1N	0 years	2.964	7.710	18.275	-1.94	2.50×10^{-3}	---	---	---	---	---	---	---	-3.33	0.105	4.015	2.47×10^{-1}
2N	1.62×10^{7}	4.275	8.100	20.024	-0.04	3.70×10^{0}	---	---	---	---	---	---	---	-1.25	0.144	4.263	1.18×10^{-1}
3N	2.52×10^{7}	5.067	8.223	21.049	2.07	5.51×10^{1}	4.968	8.227	20.920	1.63	4.90×10^{1}	0.041	0.085	0.36	0.347	4.420	7.26×10^{-2}
4N	2.90×10^{7}	5.851	7.918	22.144	15.8	3.16×10^{1}	5.079	8.282	21.094	1.72	1.29×10^{2}	0.563	0.264	1.31	0.647	4.621	4.06×10^{-2}
5N	3.00×10^{7}	5.982	7.800	22.355	24.8	1.02×10^{1}	5.034	8.264	21.026	1.65	9.33×10^{1}	0.710	0.337	1.25	0.544	4.645	3.23×10^{-2}
6N	3.20×10^{7}	6.091	7.680	22.522	37.9	2.42×10^{0}	4.971	8.183	20.902	1.92	2.69×10^{1}	0.837	0.429	0.85	0.121	4.605	2.39×10^{-2}
8N	3.55×10^{7}	6.141	7.611	22.595	52.8	8.03×10^{-1}	4.913	8.062	20.765	2.52	5.69×10^{0}	0.899	0.565	0.29	-0.391	4.519	1.97×10^{-2}
9N	7.57×10^{7}	6.180	7.478	22.654	78.5	4.69×10^{-2}	---	---	---	---	---	---	---	-1.50	-2.117	4.146	1.50×10^{-2}
10N	3.55×10^{8}	6.182	7.277	22.657	130	2.36×10^{-4}	---	---	---	---	---	---	---	-3.23	-3.057	3.922	1.43×10^{-2}
11N	2.54×10^{9}	6.182	6.875	22.657	320	6.31×10^{-10}	---	---	---	---	---	---	---	-6.81	-4.132	3.659	1.39×10^{-2}

does in fact hold for a model sequence when the temperature exponent is determined by the actual opacity law near the edge of the degenerate core.

A second comparison may be made with Schwarzschild's relation between the luminosity and the rate of decrease of the temperature of the isothermal core. If the heat content of the non-degenerate ion gas is the only source of energy, the luminosity is

$$L = -\frac{3}{2}\frac{kM}{AH}\frac{dT_c}{dt} \equiv -C\frac{dT_c}{dt}, \tag{9}$$

where C is the "heat capacity" of the entire star. Interpreting T_c as the central temperature of our models, for late phases we find that C ranges from 10 per cent larger up to as much as a factor of 3 larger than the heat capacity of the ions alone, the larger

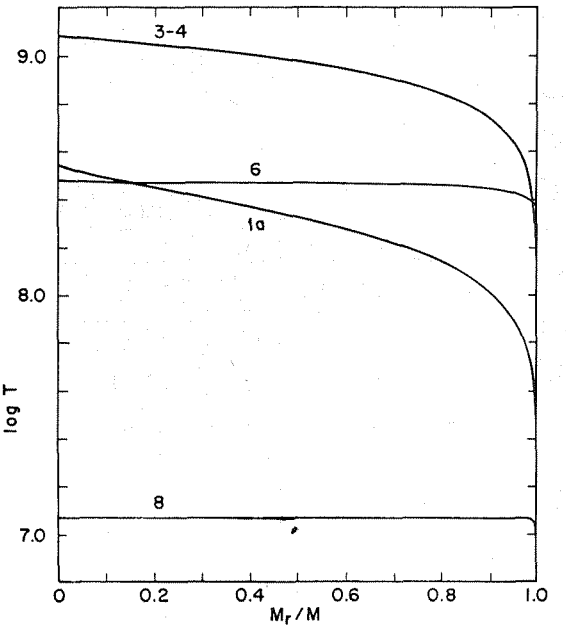

FIG. 3.—Temperature distribution as a function of fractional mass for several stages in the evolution of the 1 $M_\odot$ star without neutrino losses. Numbers refer to specific models listed in Table 1.

deviations corresponding to the smaller stellar masses. Part of this extra energy is the heat content of the electrons, while the rest is due to the small residual gravitational contraction toward the degenerate "black-dwarf" state. For the conditions appropriate to models 7–9, the ions alone supply about 70, 55, and 25 per cent of the total luminosity of the 1.0, 0.631, and 0.398 $M_\odot$ stars, respectively, while the heat content of the ions plus electrons correspondingly accounts for approximately 80, 65, and 50 per cent. Evidently our models for white dwarfs in the observed luminosity range, especially those of lower mass, are sufficiently far removed from the black-dwarf state so that the theorem of Mestel and Ruderman (1967) is not strictly applicable; gravitational contraction can still supply a fraction of the total energy release. This can have a significant effect upon the evolutionary time scales. (For a pure carbon star, of course, the effect of the electrons would be smaller by the factor $\frac{6}{26}$ than in the case of the iron stars we have studied.)

b) Evolution with Neutrino Losses

After a short period of quasi-homologous contraction a distinct difference develops between the evolution of the stellar models which include neutrino losses and those which do not. A substantial neutrino luminosity has already developed by models 2N–3N, as is evident from Tables 4–6. This has several effects.

Since these stars are essentially transparent to neutrinos, the copious generation of a large neutrino flux in these stages has the effect of "refrigerating" the stellar interior. This depresses the temperature at the center so strongly that an inverted temperature gradient is produced (Fig. 4). To supply the energy which is being lost (primarily in

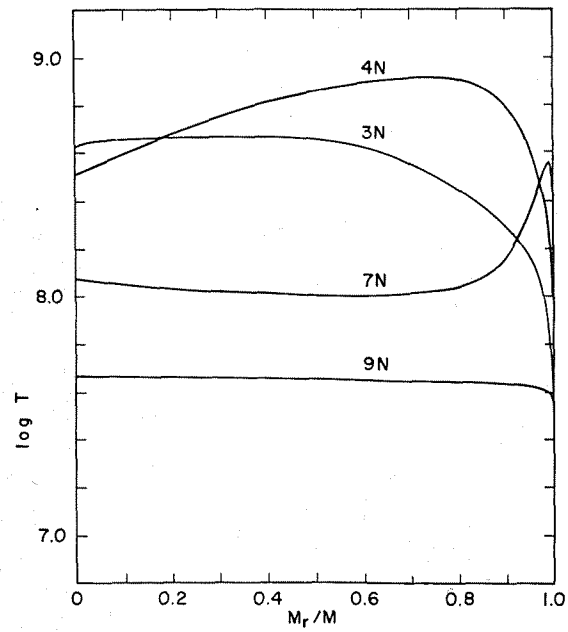

FIG. 4.—Temperature distribution as a function of fractional mass for several stages in the evolution of the 1 $M_\odot$ star with neutrino losses included. Numbers refer to specific models listed in Table 4.

the form of photoneutrinos) in these early phases of the neutrino evolution (models 3N–6N) the star must contract, and it rapidly develops an extensive, degenerate core (Fig. 5). In the contraction, the temperature at the edge of the core rises. Since the neutrino losses are confined mainly to the highly conducting, degenerate interior (Fig. 6), there is no escape route for the gravitational energy released in the non-degenerate layers, and the temperature gradient near the surface becomes appreciably steeper than in the case without neutrino loss (Figs. 3 and 4). The luminosity therefore increases considerably above the luminosity of the neutrinoless models, resulting in the upward loop in the neutrino models of Figure 1. The time scale of this loop is of the order of the time τ_ν for depletion of the thermal energy by neutrino loss:

$$\tau_\nu \sim U_\nu/\epsilon_\nu , \tag{10}$$

where U_ν is the thermal energy per gram; the fact that τ_ν is of the order of 10^4 years for the 1 $M_\odot$ star together with the proximity of the loop to the region occupied by the nuclei of the planetary nebulae in the H-R diagram (Harmon and Seaton 1964)

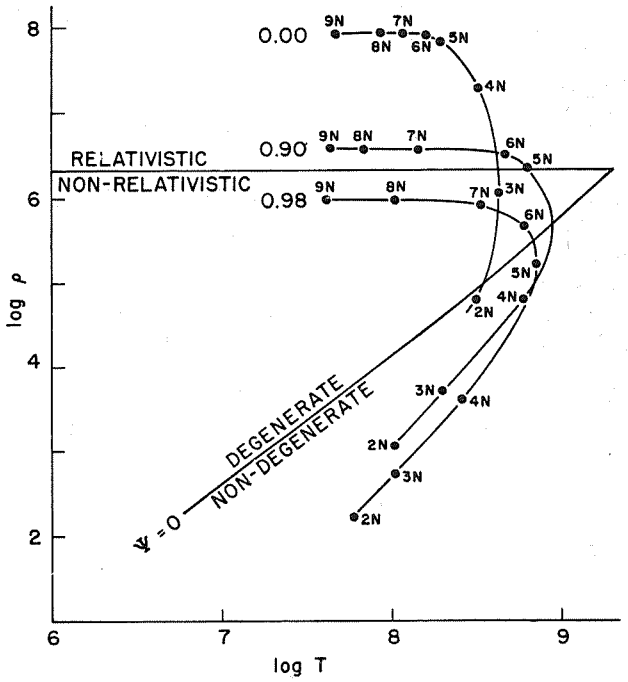

FIG. 5.—Temperature-density plane showing the evolutionary paths of several mass shells (the curves are labeled by the fractional mass M_r/M) for the 1 $M\odot$ model with neutrino losses. Degeneracy boundaries are also shown. Numbered points refer to specific models in Table 4.

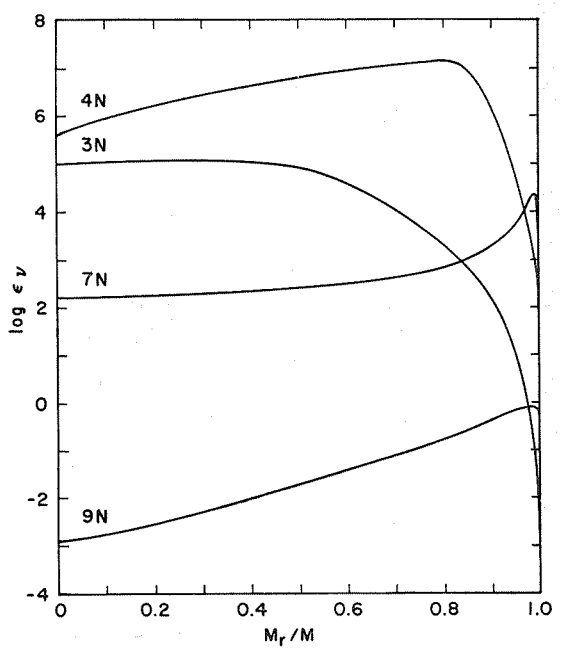

FIG. 6.—Logarithm of the total neutrino-loss rate ϵ_ν, in ergs g^{-1} sec^{-1}, as a function of the fractional mass M_r/M for the 1 $M\odot$ models with neutrino losses. Numbers refer to specific models in Table 4.

suggests that the neutrino processes in stars of mass $\sim 1\ M_\odot$ may be connected in some way with the origin of the planetary nebulae (Vila 1965, 1966).

It is of interest to estimate the range of this neutrino effect. We can estimate the maximum central temperature from the degenerate relations (Chandrasekhar 1939)

$$P_d = Af(x),\ \rho = Bx^3\ , \tag{11}$$

together with the classical relation

$$P_c = \frac{k}{\mu H}\rho T = \frac{Bx^3 kT}{\mu H} \tag{12}$$

as that temperature for which P_c equals P_d, i.e.,

$$T_{\max} = \frac{\mu H A}{kB}\frac{f(x)}{x^3} = 7.41 \times 10^8 \frac{f(x)}{x^3}\ ^\circ\mathrm{K}\ . \tag{13}$$

Empirically,

$$\begin{aligned} T_{\max} &\approx 4.5 \times 10^8 \frac{f(x)}{x^3}\ ^\circ\mathrm{K},\ \text{without neutrino losses}\ , \\ &\approx 5.6 \times 10^8 \frac{f(x)}{x^3}\ ^\circ\mathrm{K},\ \text{with neutrino losses}\ , \end{aligned} \tag{14}$$

where the constant has been chosen to be representative of the central temperature–central density relations at $T = T_{\max}$ for all our sequences.

Since the onset of degeneracy marks the end of the quasi-homologous contraction phase, we equate $T_{\max}$ to the central temperature from homologous, non-degenerate models to obtain

$$5 \times 10^8 \frac{f(x)}{x^3} \propto \frac{GM\mu H}{R}\ , \qquad \rho_c = Bx^3 \propto \frac{3M}{4\pi R^3}\ , \tag{15}$$

which determines M as a function of x and μ. Again from the models we find

$$\begin{aligned} M/M_\odot &\approx \frac{2.3}{\mu^2}\left[\frac{f(x)}{x^4}\right]^{3/2},\ \text{without neutrino losses}\ , \\ &\approx \frac{3.5}{\mu^2}\left[\frac{f(x)}{x^4}\right]^{3/2},\ \text{with neutrino losses}\ , \end{aligned} \tag{16}$$

which together with equation (14) determines the maximum central temperature as a function of the total stellar mass parametrically through the quantity x.

The range of central temperatures over which the neutrino losses dominate the evolution can be estimated in the following way. From our calculations, the photon luminosity of the neutrino models at the time of maximum central temperature is

$$L/L_\odot \approx 1300\ (M/M_\odot)^7\ . \tag{17}$$

Since the photoneutrino loss is the most important one in these early phases, the neutrino luminosity of the models should be proportional to T^8. Furthermore, the neutrino luminosity will be proportional to the mass of the neutrino-emitting core. From the models

$$L_\nu/L_\odot \approx 0.01\ (M/M_\odot)^{3/2}\ T_8{}^8\ , \tag{18}$$

where T_8 is the central temperature in units of $10^8\ ^\circ$K, and $L_\nu \propto M^{3/2}$ instead of $\propto M^1$ because the mass of the neutrino-emitting core increases more rapidly than linearly

with the total mass. The combination of equations (17) and (18) thus gives, for the central temperature at which neutrino losses will first begin to dominate the evolution, the relation

$$T_8 \gtrsim 4.4\ (M/M_\odot)^{11/16}\ . \tag{19}$$

When T_{max} from equation (14) is less than T_8 from equation (19), the neutrinos are ineffective throughout the evolution.

The rapid acceleration of the evolution by the neutrino losses is graphically illustrated in Figure 7. Since the neutrino model 1N was obtained from the sequence without neutrino losses by simply "turning on" the weak interaction, both sequences have a common model at this point (except for the neutrino losses), and acceleration of the evolution can be obtained directly from this figure. The initial spike in the luminosity at models 3N–6N is due to the photoneutrino-loss mechanism, while the plasma neutrino emission dominates the remainder of the evolution; the pair-annihilation process

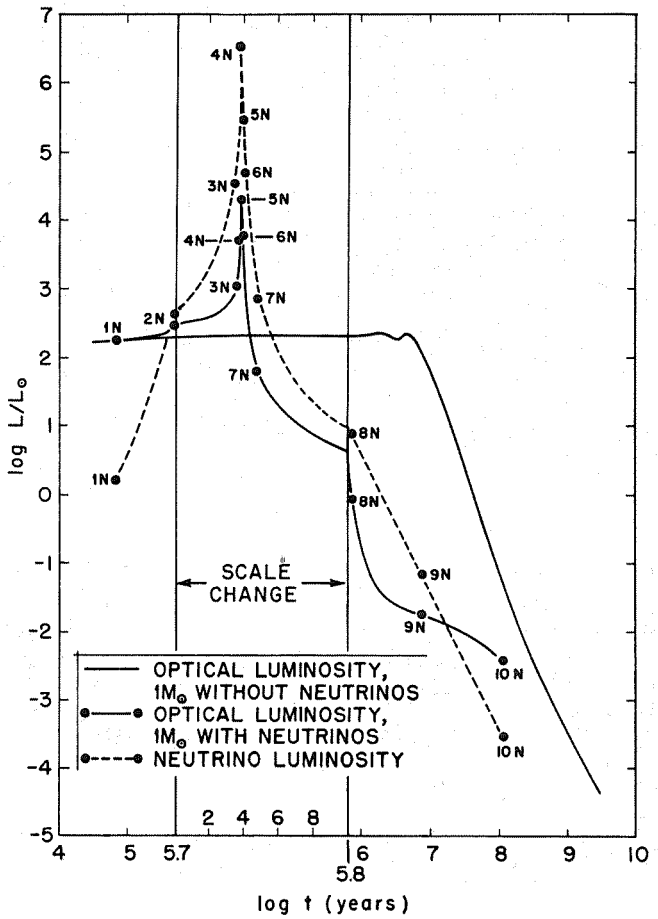

FIG. 7.—Optical and neutrino luminosities as functions of time for 1 $M_\odot$ models with and without neutrino losses. Origin of time for the neutrino models is chosen relative to a model in common with the sequence without neutrinos at an age in the latter case of 7.158×10^4 years. Note scale change between log(age) equal to 5.7 and 5.8. Numbered points refer to specific models in Table 4.

is not important in any of the models because the temperature is too low. During the plasma neutrino stage (models 7N–10N) the temperature peak produced by the neutrino losses in the core becomes sharper and moves outward toward the surface. If combustible materials were present in these layers they could be ignited at this time to produce nuclear shell burning in the outer layers, with the possibility of expulsion of material in a nebular shell.

As Figure 7 shows, the evolution of the 1 $M_\odot$ neutrino model is much more rapid than the evolution of the no-neutrino models until the optical luminosity falls to about 10^{-2} $L_\odot$. At this point the neutrino and optical luminosities are again approximately equal, and the rate of subsequent evolution is determined principally by the optical luminosity (τ_ν becomes greater than $\tau_{\rm ph}$). The temperature peak which appears so prominently in the earlier evolution now disappears, and the star is indistinguishable from the neutrinoless models. The total times required for the 0.398, 0.631, and 1 $M_\odot$ models to cool down to 10^{-2} $L_\odot$ are, respectively, 7.06×10^7, 2.20×10^7, and 2.59×10^7 years, with neutrino losses, and 4.78×10^8, 3.11×10^8, and 2.13×10^8 years, without. Thus the neutrino emission has the important effect of reducing the lifetimes of stars in the immediate pre-white-dwarf phases of evolution by about an order of magnitude!

IV. PRESUPERNOVA EVOLUTION

Burbidge *et al.* (1957) have suggested that the endoergic iron-to-helium transition, which takes place at sufficiently high temperatures in the interior of a massive star at the end of its thermonuclear evolution, can cause the implosion of the central core, followed by the explosion of the outer layers in a type II supernova outburst. This hypothesis has been elaborated by Hoyle and Fowler (1960), and numerical calculations of the implosion-explosion phase have been carried out by Colgate and White (1966), Arnett (1967), and Schwartz (1967), the latter computations including also the possibility of general-relativistic effects. Calculations of the evolution of the internal structure just prior to the core collapse have not previously been reported, however, and in this section we summarize our numerical results for this stage.

a) Evolution without Neutrino Loss

The evolutionary tracks of the presupernova models are shown in Figure 8. The initial phase consists of a homologous contraction up to model 4 where partial degeneracy sets in at the center (Fig. 9). In succeeding models gravitational-energy release increases in the outer layers, relative to the center, and the further contraction becomes less nearly homologous as degeneracy becomes increasingly important throughout the star. As is evident from Figure 9, ρ_c and T_c for our final model (5) are very close to the iron-helium transition boundary, and further evolution of the star would make it necessary to take this reaction into account.

Properties of selected models of this sequence are given in Table 7. Dynamical effects are not important for any of these models, since the rate of contraction is governed solely by the optical luminosity, which proceeds on the photon-diffusion time scale $\tau_{\rm ph} \sim 10^6$ years and is longer than either the hydrostatic readjustment time $\tau_{\rm hr} \sim (G\rho_{\rm mean})^{-1/2} \sim 10$ sec, or the evolutionary time of 3.4×10^5 years.

b) Evolution with Neutrino Losses

In the early stages of the contraction, up to model 3N, this sequence is almost identical to the one without neutrino loss. At this point, the neutrino luminosity becomes comparable to the optical luminosity, and the evolutionary tracks diverge. The optical luminosities of these models are higher than in the case without neutrinos for the reasons previously discussed in § III. In contrast to the pre-white-dwarf models, the dominant neutrino-production mechanism *throughout* the present sequence is the photo-

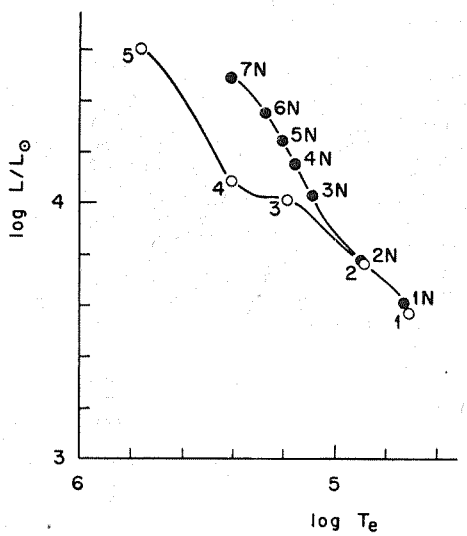

FIG. 8.—H-R diagram for pure iron stars of 2.5 $M\odot$ with neutrino losses (*filled circles* and numbers with suffix N) and without neutrino losses (*open circles* and numbers without suffix). Numbered points refer to specific models in Tables 7 and 8.

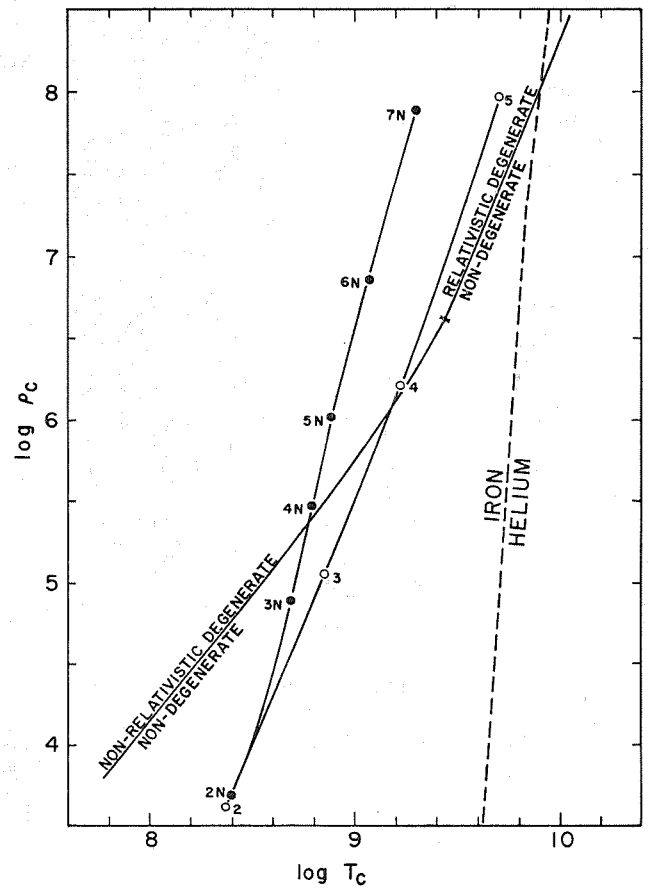

FIG. 9.—Temperature-density plane showing the evolutionary paths of the central regions for the 2.5 $M\odot$ models with and without neutrino losses. Also shown is the degeneracy boundary and the iron-helium transition line. Numbered points refer to specific models in Tables 7 and 8.

neutrino process, and there is also a significant contribution due to pair annihilation; the plasma neutrino rate is negligible outside of a very small region near the center. The high temperature dependence of the photoneutrino reaction results in a very rapid rise in the rate of energy loss, with a consequent increase in the rate of evolution of the star; in the final model, the evolutionary time scale as measured by the neutrino-loss time scale τ_ν is of the order of a few days, and the dynamical terms are of the order of 10^{-3} of the gravitational-energy release. Properties of selected models from this sequence are listed in Table 8.

In addition to accelerating the evolution, the "refrigeration" of the core by the extreme neutrino-loss rates produces a temperature inversion in the present models similar to, but less extreme than for stars below the limiting mass, as shown in Figure 10. The evolutionary track of the central region of the star in the temperature-density

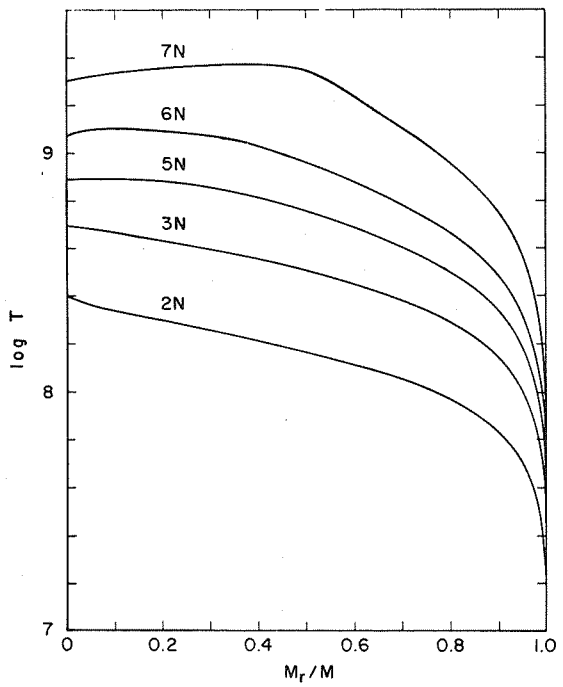

FIG. 10.—Temperature distribution as a function of fractional mass for several stages in the evolution of the 2.5 $M_\odot$ star with neutrino losses. Numbers refer to specific models in Table 8.

plane (Fig. 9) consequently begins to bend away from the iron-helium transition region; thus it is not clear whether this reaction will have any effect upon the further evolution of the core. If the further contraction proceeds along an adiabat with $\gamma = \frac{4}{3}$, the neutrino-loss time scale τ_ν, which controls the rate of evolution at this stage, becomes comparable to τ_{hr} at a temperature of about 10^{10} ° K and a density of about 10^{10} g cm^{-3}. For higher temperatures photoneutrino production alone would be sufficiently fast to initiate a free-fall collapse, in agreement with the conclusions of Chiu (1966) for a star of 10 $M_\odot$.

All of these results have been based upon the assumption that a dynamical collapse[1]

[1] Although general-relativistic effects may be important in determining the precise boundaries of the regions of dynamical instability, as discussed by Baglin (1966), the effects upon an already unstable and collapsing object appear to be negligible for densities less than 6×10^{14} g cm^{-3} (Schwartz 1967).

TABLE 7

Properties of 2.5 $M_\odot$ Models Without Neutrino Loss

No.	Age	log ρ_c	log T_c	log P_c	ψ_c	$(1-\beta)_c$	log ρ_d	log T_d	log P_d	$(1-\beta)_d$	M_d/M	r_d/R	log$L/L_\odot$	log T_e	$R/R_\odot$
1	0 years	2.738	8.083	18.495	-3.77	0.17	---	---	---	---	---	---	3.573	4.707	7.95×10^{-1}
2	2.934×10^4	3.619	8.378	19.666	-2.54	0.18	---	---	---	---	---	---	3.770	4.889	4.30×10^{-1}
3	1.048×10^5	5.049	8.857	21.591	-1.22	0.17	---	---	---	---	---	---	4.017	5.193	1.41×10^{-1}
4	2.141×10^5	6.206	9.221	23.095	+0.096	0.16	---	---	---	---	---	---	4.099	5.407	5.80×10^{-2}
5	3.411×10^5	7.973	9.713	25.458	+2.31	0.06	6.344	9.310	23.332	0.20	0.868	0.34	4.604	5.768	1.97×10^{-2}

TABLE 8

Properties of 2.5 $M_\odot$ Models With Neutrino Loss

No	Age	$\log\rho_c$	$\log T_c$	$\log P_c$	ψ_c	$\epsilon_{\upsilon,c}$	$(1-\beta)_c$	$\log\rho_{pk}$	$\log T_{pk}$	$\log P_{pk}$	ψ_{pk}	$\epsilon_{\upsilon,pk}$	$(1-\beta)_{pk}$	M_{pk}/M	r_{pk}/R	$\log L_\upsilon/L_\odot$	$\log L/L_\odot$	$\log T_e$	$R/R_\odot$
1N	0 years	2.843	8.118	18.634	-3.65	4.41×10^{0}	0.17	---	---	---	---	---	---	---	---	-0.31	3.619	4.731	7.50×10^{-1}
2N	2.852×10^{4}	3.688	8.400	19.756	2.70	7.95×10^{2}	0.18	---	---	---	---	---	---	---	---	1.94	3.783	4.903	4.10×10^{-1}
3N	5.523×10^{4}	4.880	8.699	21.232	-0.97	1.97×10^{5}	0.09	---	---	---	---	---	---	---	---	4.55	4.038	5.096	2.25×10^{-1}
4N	5.680×10^{4}	5.474	8.796	21.932	+0.20	1.21×10^{6}	0.05	---	---	---	---	---	---	---	---	5.57	4.156	5.157	1.95×10^{-1}
5N	138*	6.009	8.894	22.611	1.39	7.98×10^{6}	0.02	5.735	8.898	22.301	0.46	9.13×10^{6}	0.05	0.066	0.04	6.52	4.244	5.206	1.73×10^{-1}
6N	4.86**	6.850	9.080	23.729	3.51	3.14×10^{8}	0.01	6.295	9.099	23.066	1.08	7.14×10^{8}	0.05	0.164	0.04	8.56	4.357	5.280	1.40×10^{-1}
7N	5.43**	7.896	9.301	25.193	7.12	2.15×10^{10}	0.00	6.994	9.369	24.082	1.62	8.61×10^{10}	0.06	0.336	0.04	10.84	4.496	5.404	9.26×10^{-2}

* $+5.7\times10^{4}$ years

** $+5.716\times10^{4}$ years

will not take place before the central regions of the star reach the 50 per cent helium plus neutrons–50 per cent iron line discussed by Hoyle and Fowler (1960). Recent calculations by Rakavy, Shaviv, and Zinamon (1967) have shown, however, that the boundary of the instability region, at a given density, occurs at an appreciably lower temperature than the 50 per cent equilibrium line. Thus, while the central temperature of 10^{10} ° K extrapolated from our models is still 20 per cent less than the temperature required to dissociate half of the iron into helium plus neutrons at the extrapolated central density of 10^{10} g cm^{-3}, it appears to be sufficient to drive the central regions of the star well into the region of dynamical instability. On the other hand, the calculations of the iron-helium transition instability have all been based upon the assumption of strict thermodynamic equilibrium, while it is actually the *rate* of this dissociation reaction which determines which mechanism is the cause of the instability in the borderline cases. Since the rate of this reaction has never been accurately calculated, and since in addition the pair-annihilation and photoneutrino rates which we have used overestimate the rate of energy loss under these extreme conditions, we cannot predict accurately the stellar mass at which the iron-helium transition becomes the mechanism responsible for the collapse. We note that Fowler and Hoyle (1964) recently emphasized that this transition must be the cause of the implosion of the core in sufficiently massive stars.

Finally, let us compare our models with the starting models used by Colgate and White (1966). Their initial (2 $M_\odot$) model consisted of a polytrope ($n = 3$, $\rho_c = 9.5 \times 10^8$ g cm^{-3}) with pair annihilation and URCA-process neutrino losses. The initial contraction of this model approximated an adiabat with $\gamma = \frac{4}{3}$, up to a density of about 2×10^{10} g cm^{-3}, where electron capture rapidly converted the iron into neutron matter. The iron-helium transition did *not* occur in this model sequence.

In our final model with the central density of 7.9×10^7 g cm^{-3}, the central temperature of 2×10^9 ° K is already considerably depressed by both electron conduction and neutrino losses below the value of 3.4×10^{10} ° K which would be appropriate to a 2. $M_\odot$ polytrope with $n = 3$. Since the neutrino losses increase much more rapidly with temperature than does the gravitational-energy production, a polytropic starting model may not be adequate for the supernova calculations. Furthermore, since the photoneutrino-loss rate is dominant in these phases, the central regions may be driven even farther away from the iron dissociation region than in Colgate and White's models. Both of these effects will affect the precise mass limit at which the neutrino losses cease to be the cause of the core collapse. Further, Colgate and White's work showed that in this stage the model contracts along an adiabat with $\gamma = \frac{4}{3}$. Despite the non-polytropic structure for our models, we find that the central pressures can be approximated by a power law $P_c \propto \rho_c^{1.34}$, thus confirming this aspect of their calculation.

V. SUMMARY AND CONCLUSIONS

The principal results of this study may be summarized as follows.

i) For the three models with mass less than the Chandrasekhar limit and without the inclusion of the neutrino processes, the energy released in the white-dwarf phases ($\log L/L_\odot \sim -2$ to -4) is derived partly from gravitational contraction as well as from the heat loss of the ions *plus* electrons. For the stars of lower mass, gravitational-energy release supplies a larger fraction of the total energy than in stars of mass $\sim 1\ M_\odot$, indicating that the degree of degeneracy in these stars is not yet sufficiently large for strict applicability of extrapolations from the black-dwarf state. Such considerations are useful as a first approximation, however.

ii) As mentioned by Schwarzschild (1958, p. 237), a power-law relation between the luminosity of a white dwarf and the temperature at the edge of the degenerate core does exist although the temperature exponent (which is determined by the tempera-

ture dependence of the opacity law) is somewhat less than the value of 3.5 derived by Schwarzschild from Kramers' law. White dwarfs without neutrino losses consequently spend more time in a given range of luminosities than expected on the basis of the analytic model.

iii) Inclusion of neutrino losses accelerates the rate of evolution, since energy losses proceed on the neutrino time scale τ_ν rather than on the time scale for photon diffusion. The increased energy losses effectively refrigerate the central regions of the star and produce a temperature inversion with a peak just outside the edge of the degenerate core. The steepening of the temperature gradient in the outer layers which then results produces a higher luminosity in the neutrino models, which consequently traverse loops in the H-R diagram at fairly high luminosities before strong degeneracy sets in

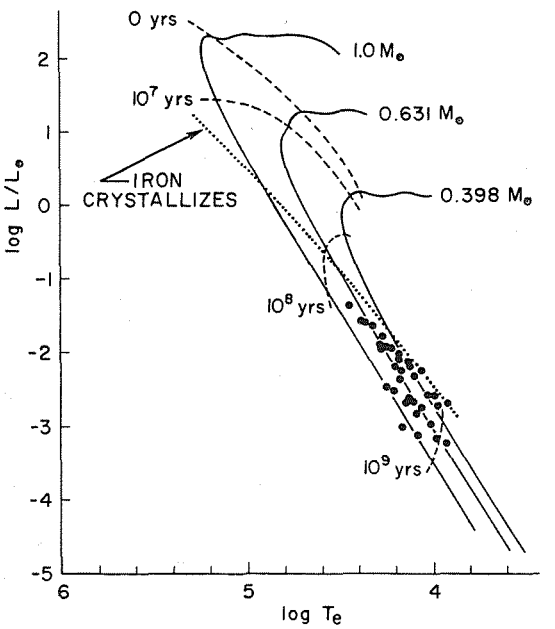

FIG. 11.—Isochrons for pre-white-dwarf models without neutrino losses. Times are measured from epoch of maximum optical luminosity.

The similarity of the position and time scale of the loop in the case of the 1 $M_\odot$ star to the evolutionary track found by Harmon and Seaton (1964) for the nuclei of the planetary nebulae suggests the possibility that the nebular expulsion may result from the triggering of thermonuclear reactions in the outer layers of the star when combustible material is traversed by the temperature peak (Kutter 1968; Savedoff, Kutter, and Van Horn 1968).

iv) In the immediate pre-white-dwarf phases, the lifetimes of the neutrino models are about an order of magnitude smaller than for the no-neutrino models. These results agree somewhat better with the available observations of the statistics for the hottest white dwarfs than do the models without neutrino losses. This supports the suggestion (Chin, Chiu, and Stothers 1966; Stothers 1966) that the apparent lack of stars immediately above the region of the H-R diagram occupied by the white dwarfs may be due to these neutrino processes; however, the statistics are not yet adequate for a decisive test of the weak-interaction theory. Isochrons have been plotted into the (log L, log T_e)-

plane as well as evolutionary tracks for these models in Figures 11 and 12. The observational points are taken from Eggen and Greenstein (1965). Because of the probable importance of crystallization (Van Horn 1968) a detailed comparison with the observations seems unwarranted at this time. It should be noted that before the model crosses the crystallization line the isochrons constitute a lower limit to the age difference from maximum luminosity. Only in the extreme crystal region should the specific heat vitiate these lower limits (Ostriker 1968).

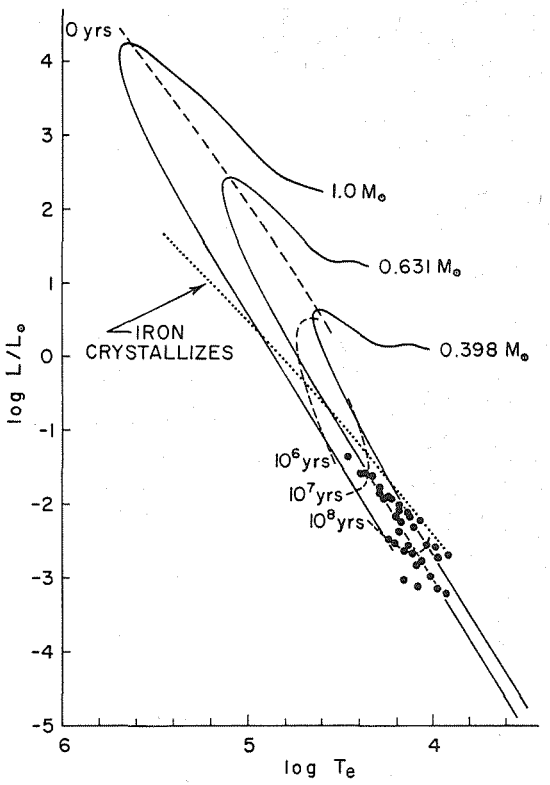

FIG. 12.—Isochrons for pre-white-dwarf models with neutrino losses included. Times are measured from the epoch of maximum optical luminosity.

v) Presupernova models of $2.5^{*}M_{\odot}$ have been followed to the iron-helium transition or to the point at which the dynamical effects cannot continue to be neglected. In the neutrinoless models, the evolution proceeds by quasi-homologous contraction up to the boundary of the iron-helium transition zone.

vi) In the neutrino models, the depression of the central temperature by the photoneutrino process appears to prevent the iron-helium transition from occurring, in agreement with the results found by Chiu (1966) and by Colgate and White (1966) for stars of sufficiently low mass. If no other physical processes intervene, the photoneutrino loss appears to be capable of initiating a core collapse at a temperature of $\sim 10^{10}$ ° K and a density of $\sim 10^{10}$ g cm^{-3}. However, the photoneutrino rates which we have used overestimate the loss rates in regions of such strong degeneracy, and future calculation must use more realistic estimates for these rates (Beaudet, Petrosian, and Salpeter

1967). Further work is also needed on the dissociation rate for iron in regions of strong degeneracy before the precise mechanism responsible for the core collapse in a supernova model of given mass can be definitely established.

This work was begun by S. Vila as his thesis at Rochester. We have benefited immeasurably from the guidance and advice of H. L. Helfer, and we are grateful to M. Schwarzschild for providing us with his program for stellar-evolution calculations which we have adapted for these calculations. One of us (M. P. S) wishes to express his gratitude to Professor J. H. Oort for his hospitality during the time spent at the Leiden Observatory and to the cooperation of M. J. Seaton of the University of London and the Computer Center of Imperial College, London. This work has been supported in part by the Air Force Office of Scientific Research under grant AF 603-64 and in part by the National Science Foundation under grant GP-6174.

REFERENCES

Arnett, D. 1967, *Canadian J. Phys.*, **45**, 1621.
Baglin, A. 1966, *Ann. d'ap.*, **29**, 103.
Beaudet, G., Petrosian, V., and Salpeter, E. E. 1967, *Ap. J.*, **150**, 979.
Bodenheimer, P. 1966, *Ap. J.*, **144**, 709.
Burbidge, E. M., Burbidge, G., Fowler, W. A., and Hoyle, F. 1957, *Rev. Mod. Phys.*, **29**, 547.
Chandrasekhar, S. 1939, *Stellar Structure* (Chicago: University of Chicago Press), p. 412.
Chin, C.-W., Chiu, H.-Y., and Stothers, R. 1966, *Ann. Phys.*, **39**, 280.
Chiu, H.-Y. 1966, in *Stellar Evolution*, ed. R. F. Stein and A. G. W. Cameron (New York: Plenum Press), p. 279.
Colgate, S., and White, R. 1966, *Ap. J.*, **143**, 626.
Eggen, O. J., and Greenstein, J. L. 1965, *Ap. J.*, **141**, 83.
Feynman, R. P., and Gell-Mann, M. 1958, *Phys. Rev.*, **109**, 193.
Fowler, W. A., and Hoyle, F. 1964, *Ap. J. Suppl.*, **9**, 201.
Grasberger, W. H. 1961, U.C.R.L. Rept. No. 6196.
Harmon, R. J., and Seaton, M. J. 1964, *Ap. J.*, **140**, 824.
Härm, R., and Schwarzschild, M. 1964, *Ap. J.*, **139**, 594.
Hayashi, C., Hōshi, R., and Sugimoto, D. 1962, *Suppl. Progr. Theoret. Phys. Japan*, No. 22.
Henyey, L. G., Forbes, J. E., and Gould, N. L. 1964, *Ap. J.*, **139**, 306.
Henyey, L. G., Wilets, L., Böhm, K.-H., LeLevier, R., and Levée, R. D. 1959, *Ap. J.*, **129**, 628.
Hoyle, F., and Fowler, W. A. 1960, *Ap. J.*, **132**, 565.
Inman, C. L., and Ruderman, M. A. 1964, *Ap. J.*, **140**, 1025.
Kutter, G. S. 1968, unpublished Ph.D. thesis, University of Rochester.
Mestel, L. 1950, *Proc. Cambridge Phil. Soc.*, **46**, 331.
Mestel, L., and Ruderman, M. A. 1967, *M.N.R.A.S.*, **136**, 27.
Ostriker, J. P. 1968, *A.J.*, **73**, S31.
Rakavy, G., Shaviv, G., and Zinamon, Z. 1967, *Ap. J.*, **150**, 131.
Savedoff, M. P., Kutter, S. G., and Van Horn, H. M. 1968, *I.A.U. Symp. No. 34* ed. D. E. Osterbrock and C. R. O'Dell (Dordrecht: D. Reidel Publishing Co.), p. 400.
Salpeter, E. E. 1961, *Ap. J.*, **134**, 669.
Schwartz, R. 1967, *Ann. Phys.*, **43**, 42.
Schwarzschild, M. 1958, *Structure and Evolution of the Stars* (Princeton, N.J.: Princeton University Press).
Stothers, R. 1966, *A.J.*, **71**, 943.
Sudarshan, E. C. G., and Marshak, R. E. 1958, *Phys. Rev.*, **109**, 1860.
Van Horn, H. M. 1968, *Ap. J.*, **151**, 227.
Vila, S. C. 1965, unpublished Ph.D. thesis, University of Rochester.
———. 1966, *Ap. J.*, **146**, 437.
Zaidi, M. H. 1965, *Nuovo Cimento*, **40**, 502.